Low-Loss Unidirectional Acoustic Focusing Transducer in Thin-Film Lithium Niobate

Ruochen Lu, *Member, IEEE*, Yansong Yang, *Member, IEEE*, and Songbin Gong, *Senior Member, IEEE*

***Abstract*— In this work, we present gigahertz low-loss unidirectional acoustic focusing transducers in thin-film lithium niobate. The design follows the anisotropy of fundamental symmetric (S0) waves in X-cut lithium niobate. The implemented acoustic delay line testbed consisting of a pair of the proposed transducers shows a low insertion loss of 4.2 dB and a wide fractional bandwidth of 7.5% at 1 GHz. The extracted transducer loss is 1.46 dB, and the propagation loss of the S0 waves is 0.0126 dB/μm. The design framework is readily extendable to other acoustic modes, given consideration on the optimal orientation for power flow and electromechanical transduction.**

***Index Terms*— Acoustic delay line (ADL), lithium niobate, microelectromechanical systems (MEMS), piezoelectricity, power flow angle, S0 mode, wave focusing transducer.**

I. Introduction

FOCUSING of radio frequency (RF) acoustic waves on-chip has been a popular topic of research due to its potential applications in RF signal processing [1]–[6], sensing or actuation [7]–[11], optomechanical or photoelastic transductions [12]–[16], and quantum electromechanical systems [17]–[20]. From a signal processing perspective, wave focusing allows the frequency-selective transformation of impedances and directional coupling between the input and the output [1]–[3], which can find use in RF front ends. From an energy perspective, it allows the reduction of modes [20], the focus of power [7], and efficient waveguiding to enhance the cross-domain interaction between the phonons and other physics of interest [17]–[19].

Similar motivations are also behind the development of chip-scale wave focusing structures in photonics where periodic reflective gratings are made for this purpose [21]–[24]. Unfortunately, the techniques in chip-scale light focusing, despite being inspirational, are not directly translatable to acoustics. Different from its photonic counterpart, acoustic focusing often requires piezoelectric transduction embedded with concurrent unidirectionality [25] and a focusing mechanism, while carefully navigating the anisotropy of the media [12]. Moreover, the cross-domain systems require efficient transduction mechanism or material for wideband access of the acoustic domain [16], [26]. Such demanding requirements underline the bottlenecks that have stymied the use of wave focusing in the chip-scale acoustic systems.

Recently, advances in single-crystal thin-film transfer techniques [27] enable the thin-film lithium niobate ($LiNbO_3$) platform [28], offering an opportunity to address the challenges above simultaneously. Its advantages can be enumerated as follows. First, an assortment of the acoustic modes with large electromechanical coupling (K^2) can be excited in thin-film $LiNbO_3$ [29]–[31], for example, fundamental symmetric (S0) [32]–[36], fundamental shear horizontal (SH0) [37]–[41], and first-order antisymmetric (A1) modes [42]–[45]. They permit much wider bandwidth transduction between the acoustic and electrical domains than the state-of-the-art at RF. Second, the reported low electrical [46] and mechanical damping [47], [48] at RF promises lower loss. Third, one can enable gigahertz operating frequencies with large feature sizes due to the fast phase velocities of plate waves [31]. Finally, thin-film $LiNbO_3$ also possesses desired electrooptic and photoelastic properties for optomechanical and quantum electromechanical systems [16], [26]. Exploiting these advantages, researchers have demonstrated both resonant [49] and nonresonant [41], [50] devices with unprecedentedly large fractional bandwidth (FBW) and low insertion loss (IL). However, studies on efficient acoustic focusing transducers in thin-film $LiNbO_3$ have not been done.

This work produces unidirectional focusing transduction of the S0 mode in X-cut thin-film $LiNbO_3$. To do so, we exploit the above advantages of $LiNbO_3$ without being spoiled by its complex anisotropy. The design herein uses single-phase unidirectional transducers (SPUDTs) arranged in the orientation with the maximum K^2 and also curved according to the dependence of the phase velocity on orientation. The proposed design is then validated with the acoustic delay line (ADL) testbeds using the unidirectional transducers. The testbed shows a low IL of 4.2 dB and a wide FBW of 7.5% at 1 GHz. The extracted transducer loss is 1.46 dB, and the propagation loss (PL) of S0 is 0.0126 dB/μm. Note that although our designs are specific to S0, the design can be modified and translated to other modes [34], [44], given consideration on the optimal orientation for power flow and electromechanical transduction.

Manuscript received March 27, 2020; accepted July 21, 2020. Date of publication July 23, 2020; date of current version November 23, 2020. This work was supported by the Defense Advanced Research Projects Agency (DARPA) Microsystems Technology Office Near Zero Power RF and Sensor Operations (NZERO) and Signal Processing at RF (SPAR) Programs. *(Corresponding author: Ruochen Lu.)*

The authors are with the Department of Electrical and Computing Engineering, University of Illinois at Urbana–Champaign, Urbana, IL 61801 USA (e-mail: rlu10@illinois.edu).

Digital Object Identifier 10.1109/TUFFC.2020.3011624

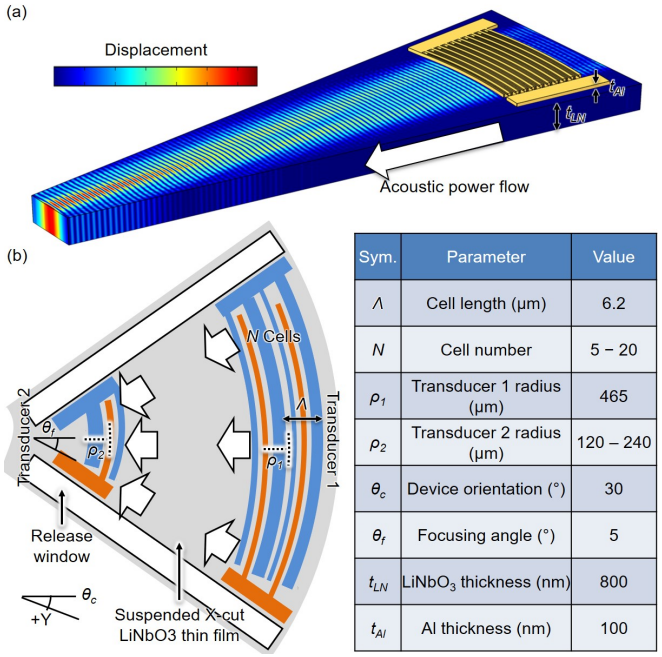

Sym.	Parameter	Value
Λ	Cell length (μm)	6.2
N	Cell number	5 – 20
ρ_1	Transducer 1 radius (μm)	465
ρ_2	Transducer 2 radius (μm)	120 – 240
θ_c	Device orientation (°)	30
θ_f	Focusing angle (°)	5
t_{LN}	$LiNbO_3$ thickness (nm)	800
t_{Al}	Al thickness (nm)	100

Fig. 1. (a) Simulated vibrational mode shape of the proposed unidirectional acoustic focusing transducer using S0 in thin-film $LiNbO_3$. (b) Schematic of the ADL testbed with a pair of acoustic focusing transducers. Key design parameters are listed in the inset table.

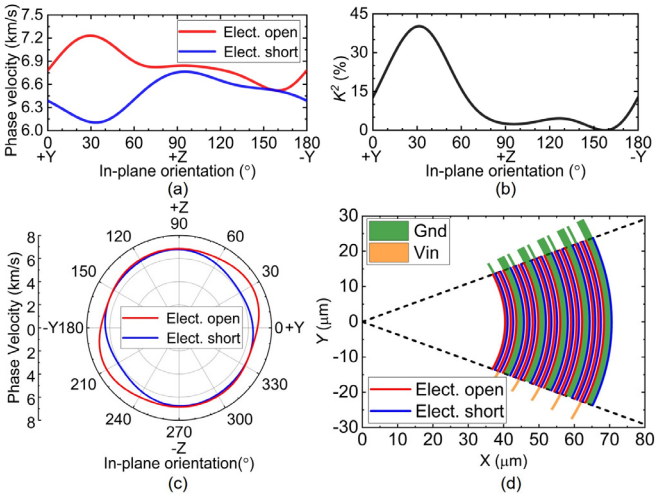

Fig. 2. (a) Phase velocities of S0 under the electrically open and short boundary conditions. (b) Piezoelectric coupling coefficient of S0 at different in-plane orientations. (c) Phase velocity in-plane anisotropy of the S0 waves. (d) Design example of the curved transducers with a focusing angle (θ_f) of 20°.

This article is organized as follows. Section II first introduces the design of a unidirectional acoustic focusing transducer and its ADL testbeds. Section III presents the fabricated devices. Section IV shows the measured data and the extracted transducer loss (TL). Finally, the conclusion is stated in Section V.

II. Design and Simulation

A. Overview of Unidirectional Acoustic Focusing Transducer

The mockup view of the unidirectional acoustic focusing transducer is shown in Fig. 1(a). The device is composed of 100-nm aluminum (Al) interdigitated electrodes on the top of an 800-nm suspended X-cut $LiNbO_3$ thin film. The SPUDT design is implemented to eliminate the 6-dB bi-directional loss [25]. The SPUDT consists of cascaded arch-shaped cells with each cell having a length of Λ. Each cell includes a pair of $\Lambda/8$ wide nonreflective interdigitated electrodes and a $3\Lambda/8$ wide nontransductive reflector. Their asymmetric placement in the cell leads to constructive interference between the directly transduced and reflected waves in the forward direction and destructive interference in the backward direction. With adequate transducer cells cascaded, unidirectional wave transduction can be achieved. The SPUDT is also curved toward the focusing point based on the anisotropic velocity of S0. In operation, the alternating electric fields between the electrodes generate the S0 waves through piezoelectricity. The generated acoustic wave unidirectionally propagates toward the focus [see Fig. 1(a)].

To directly capture the wave focusing effect within the electrical domain, the ADL testbeds are designed with a pair of the proposed transducers facing each other on the opposite ends of the acoustic waveguide [see Fig. 1(b)]. The electrical energy is converted into the acoustic domain at the input transducer (Transducer 1), which propagates toward the output transducer (Transducer 2) before converting back into the electrical domain. A fan-shaped acoustic waveguide, defined by the etch windows, is used as an example. The effectiveness of the focusing transducer design is evaluated by the ADL testbeds with different waveguide shapes, for example, fan-shaped and rectangular waveguides. If testbeds with the same transducer but different waveguides have the same S-parameters, the design can be validated. The key parameters and the typical values are listed in the inset table. More details on the design parameters will be discussed in Sections II-B and II-C.

B. Design of Unidirectional Acoustic Focusing Transducer

The unidirectional acoustic focusing transducer is based on the reported gigahertz S0 SPUDT transducers [34]. Different from the S0 ADLs, which only use acoustic wave propagation at the orientation with the maximum K^2, the in-plane anisotropy of S0 plays an essential role in focusing transducers, both in terms of transduction and propagation.

The in-plane S0 characteristics are first studied using the 2-D eigenmode finite element analysis (FEA) [34]. An X-cut $LiNbO_3$ plate with a Λ of 6.2 μm and a thickness of 0.8 μm is studied at different in-plane orientations. These dimensions are selected for efficient S0 transduction at 1 GHz [34]. Periodic mechanical and electrical boundary conditions are applied to the vertical edges. The mechanical free boundary conditions are applied to the top and the bottom surface. The phase velocities of S0 under the electrical open and short conditions are shown in Fig. 2(a). The velocities under the electrically open condition are faster due to the piezoelectric stiffening effect [51], with a maximum velocity of 7.2 km/s at 30° to the

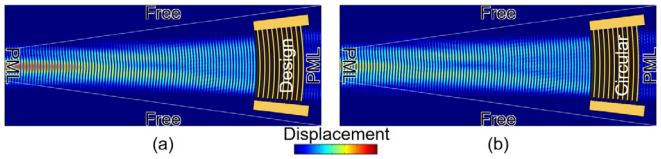

Fig. 3. Simulated vibrational mode shape of (a) proposed focusing transducer and (b) circular transducer within a rectangular waveguide.

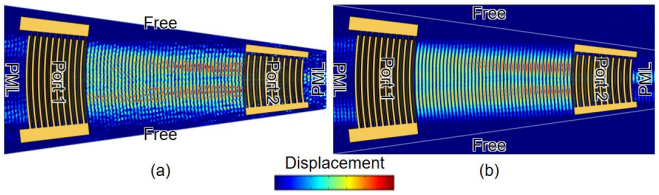

Fig. 4. Simulated vibrational mode shape of the ADL testbeds with (a) fan-shaped and (b) rectangular waveguide.

Y-axis. Based on such a velocity difference, K^2 is calculated as $[(v_{\text{open}}/v_{\text{short}})^2-1]$ [29] and plotted in Fig. 2(b), showing a maximum value of 40% also at 30° to the Y-axis.

The focusing transducer is then designed accordingly. First, to yield the most efficient piezoelectric transduction, the orientation of the transducer is centered at 30° to the Y-axis. Second, to compensate for the anisotropy of S0, the transducers are curved based on the phase velocity in-plane anisotropy [see Fig. 2(c)], instead of a circular pattern drawn from the focus point. Such a design can be better rationalized by examining the reverse process, namely, a point acoustic source at the focus point launching waves toward SPUDT. To align the transducers with the constant phase front, the transducer sections on the sides have to bent further inward to accommodate the slower velocities at orientations deviating from 30° to the Y-axis. Different velocities for the parts with and without electrodes are accounted for by aggregating the phase delays across the different sections at their respective phase velocities. Following the procedure, an example of curved transducers with a one-side focusing angle (θ_f) of 20° is designed and shown in Fig. 2(d). Such a θ_f is used to illustrate the curvature. The electrodes are then connected to either ground or signal, following the SPUDT design.

The frequency-domain FEA is performed to validate the focusing transducer design (see Fig. 3). The simulation includes the suspended $LiNbO_3$ thin film and the patterned electrodes. The transducer design has a θ_f of 5°, and a central transducer radius (ρ) of 465 μm. θ_f of 5° is selected as an example. Following the approach, transducers with different θ_f can be designed for various applications. The mechanical free boundary conditions are applied to the release windows. The perfectly matched layers (PMLs) are applied in the boundaries along the wave propagation direction for removing multireflections. Unidirectional transduction can be observed. The proposed design [see Fig. 3(a)] achieves a more concentrated acoustic beam than the circular one [see Fig. 3(b)].

Note that for different acoustic microsystems, the design approach in Section II-B can be applied to efficiently excite and focus other acoustic modes in $LiNbO_3$, such as SH0 [40] and A1 [44], using the corresponding in-plane properties.

C. Design of ADL Testbeds

The ADL testbeds, consisting of a pair of focusing transducers, are implemented to validate the transducer design. As explained in Section II-A, the testbeds with the same transducer design but different waveguides will be used for checking whether acoustic energy fails to focus and leaks to the side.

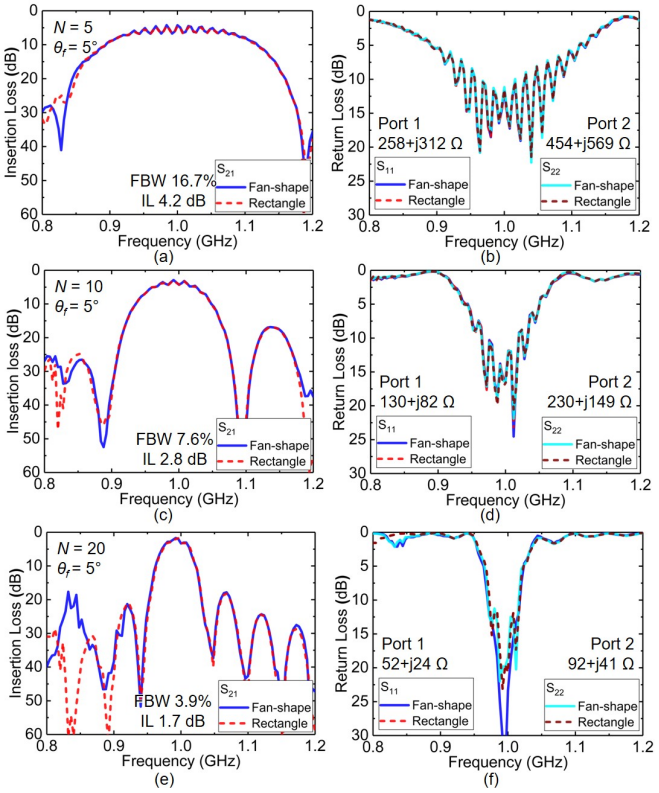

Fig. 5. Simulated (a) IL and (b) RL of the testbeds with an N of 5. Simulated (c) IL and (d) RL of the testbeds with an N of 10. Simulated (e) IL and (f) RL of the testbeds with an N of 20.

The testbed ADLs are studied as an example (see Fig. 4), with a Λ of 6.2 μm, a θ_f of 5°, a cell number (N) of 10, and a radius of 465 μm for Transducer 1 (ρ_1) and 240 μm for Transducer 2 (ρ_2). Both the fan-shaped [see Fig. 4(a)] and rectangular [see Fig. 4(b)] waveguides are simulated using the frequency-domain FEA. The simulation assumes lossless conditions. The free boundary conditions are applied to the side of the waveguides, and the PMLs are placed on the ends along the wave propagation direction. The vibrational mode shape shows that the acoustic energy is concentrated between the transducers, validating the unidirectional design. The acoustic waves are focused by the transducer, showing a larger amplitude near Transducer 2. The mode shapes for both the cases are similar, except for the slight difference due to diffraction.

The testbeds with N of 5 and 20 are also simulated for exploring the IL-FBW design space. Devices with different N have the same central transducer positions. The IL and return

TABLE I
KEY PARAMETERS OF THE FABRICATED DEVICES

Index	Λ (μm)	θ_f (°)	ρ_1 (μm)	ρ_2 (μm)	N	Comments
Group A	6.2	5	465	240	5 – 20	IL-FBW Trade-off & Focusing Validation
Group B	6.2	5	465	120 – 240	10	TL & PL

loss (RL) of different devices are plotted in Fig. 5, with both ports conjugately matched. The five-cell device has an IL of 4.2 dB over a 3-dB FBW of 16.7% [see Fig. 5(a) and (b)]. The ten-cell device has an IL of 2.8 dB over a 3-dB FBW of 7.6% [see Fig. 5(c) and (d)]. The 20-cell device has an IL of 1.7 dB over a 3-dB FBW of 3.9% [see Fig. 5 (e) and (f)]. Transducers with more cells achieve lower IL at the cost of smaller FBW, described as the IL-FBW tradeoff [34]. The IL-FBW design tradeoff originates from the finite reflectivity per wavelength in high K^2 substrates [25], [34]. Another effect of the limited reflectivity is the in-band ripples caused by the multi-transit echoes. S0 in thin-film $LiNbO_3$ shows significantly lowered IL over much wider FBW when compared with the conventional acoustic platforms, thanks to the much larger K^2 and the thin-film structure [34]. The IL and RL of the devices with different waveguide shapes are also compared in Fig. 5. Thanks to the transducer design, the in-band performance of different waveguides shows little difference, validating that the S0 waves are focused and do not leak into the waveguide section on the sides.

To sum up, unidirectional acoustic focusing transducers are designed by adjusting the S0 SPUDT design based on the in-plane anisotropy of S0, considering both the wave transduction and propagation. The design is validated by FEA using the ADL testbeds, showing record-low IL over wide FBW.

III. IMPLEMENTATION

The devices are in-house fabricated following the fabrication process reported in [34]. An 800-nm X-cut $LiNbO_3$ thin film on a 4-in Si wafer is provided by NGK Insulators, Ltd., for the fabrication. The top 100-nm Al electrodes are sputtered first. Next, SiO_2 is deposited as the hard mask for etching $LiNbO_3$. Then, the release windows are defined using inductively coupled plasma reactive ion etching. The devices are finally released by XeF_2-based Si etching.

The optical images of the implemented devices are presented in Fig. 6, with the critical parameters labeled. For the design simulated in Section II-C, the zoomed-out [see Fig. 6 (a)] and the zoomed-in images of both the focusing transducers [see Fig. 6 (b) and (c)] show well-defined transducers and fan-shaped acoustic waveguides. The reference device with identical transducers but a rectangular waveguide is presented in Fig. 6(d).

Two groups of devices were fabricated (see Table I). The devices in Group A have the same cell width and the same transducer position, but different N of 5, 10, and 20. These devices are intended for exploring the IL-FBW tradeoff of the unidirectional focusing transducer design. Moreover, designs with fan-shaped and rectangular waveguides were

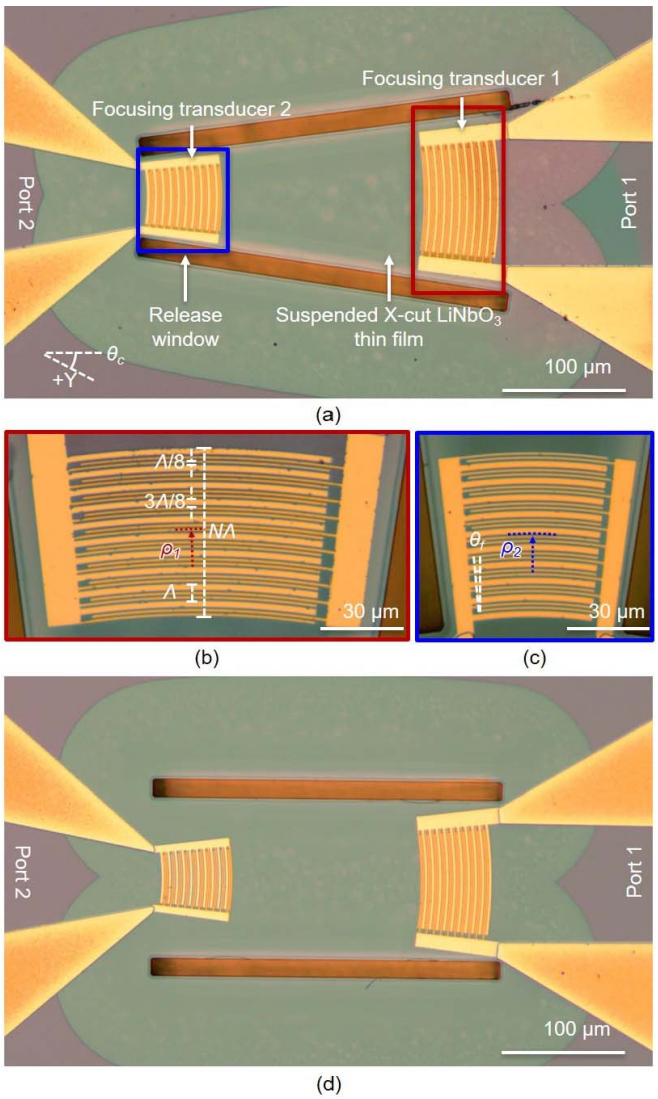

Fig. 6. Optical microscope image of (a) ADL testbed with a pair of unidirectional acoustic focusing transducers within a fan-shaped waveguide. Zoomed-in image of (b) Port 1 and (c) Port 2. (d) ADL testbed with a rectangular waveguide.

implemented for all the devices for validating the design. The devices in Group B have the same transducer design, but different gap lengths ($\rho_1 - \rho_2$). They are used for extracting the TL of the transducer pair and PL of S0.

IV. MEASUREMENTS AND DISCUSSION

A. ADL Testbeds With Different Cell Numbers

The fabricated ADL testbeds were first measured with a Keysight N5249A vector network analyzer (VNA) at a −10-dBm power level in air, and then conjugately matched in Keysight Advanced Design System (ADS).

The performance of the devices in Group A is plotted in Fig. 7. The testbeds with different N and waveguide shapes are measured. The five-cell device has an IL of 5.6 dB over a 3-dB FBW of 17.3% [see Fig. 7(a) and (b)]. The ten-cell device has an IL of 4.2 dB over a 3-dB FBW of 7.5% [see Fig. 7(c) and (d)]. The 20-cell device has an IL of 3.8 dB over

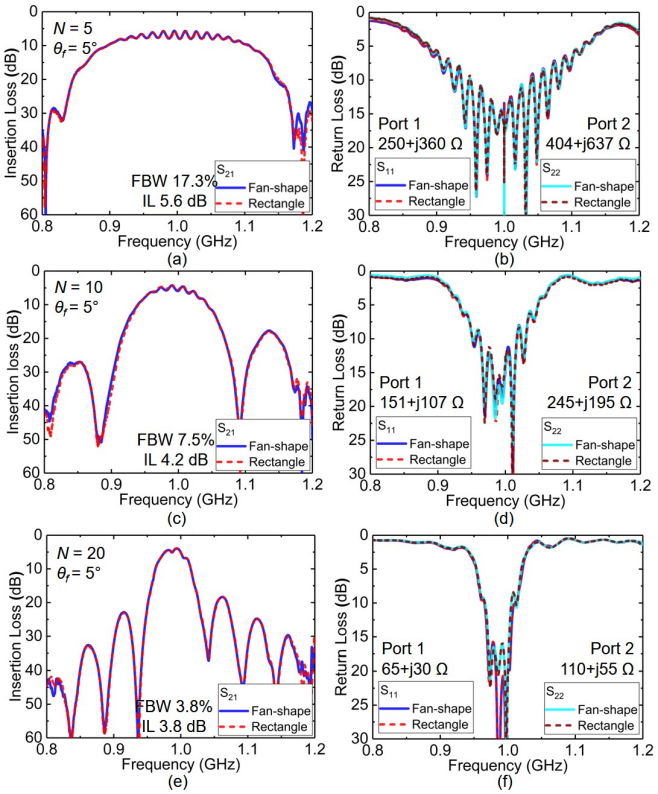

Fig. 7. Measured (a) IL and (b) RL of the testbeds with an N of 5. Measured (c) IL and (d) RL of the testbeds with an N of 10. Measured (e) IL and (f) RL of the testbeds with an N of 20.

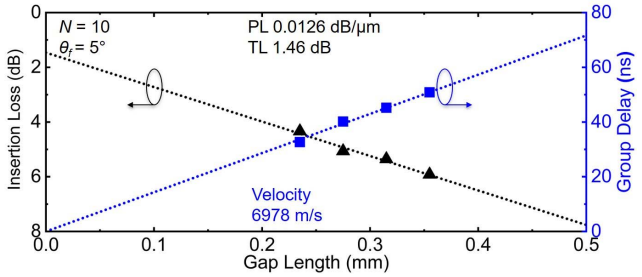

Fig. 8. IL and delay of the ADL testbeds with different gap lengths. The extracted TL is 1.46 dB, and the PL is 0.0126 dB/μm. The extracted velocity of S0 is 6978 m/s.

a 3-dB FBW of 3.8% [see Fig. 7(e) and (f)]. The measured 3-dB FBW matches well with the simulated results, and additional IL around 1.6 dB is observed, which is the PL introduced by mechanical and electrical damping in addition to wave diffraction during the focusing process. The results show significant improvement in terms of the IL-FBW design space, when compared with the conventional acoustic platforms [1]. Moreover, the results with different waveguide shapes are also plotted in Fig. 7, showing a minimum difference for the S0 passband. The results validate the unidirectional focusing transducer design.

B. ADL Testbeds With Different Gap Lengths

The devices in Group B are also measured in air and then conjugately matched with ADS. The obtained IL and in-band group delays are plotted in Fig. 8, for different gap lengths. The extracted PL is 0.0126 dB/μm, and the obtained velocity for S0 is 6978 m/s, both agreeing with the reported values for S0 at 1 GHz [34]. The extracted PL is much higher than the surface acoustic waves in YZ $LiNbO_3$ (0.0002 dB/μm) [52], likely due to the surface effects introduced when micromachining the thin film [53]. The extrapolated TL for a pair of unidirectional focusing transducers is 1.46 dB. Such TL originates from the insufficient unidirectionality of the ten-cell design. Upon further optimizations, the TL can be further improved by placing more cells, which is at the cost of narrower FBW, or using thicker electrodes for more efficient reflectors.

This article presents the design fundamentals and the implementation of low-loss acoustic focusing transducers in high K^2 thin-film $LiNbO_3$ platforms. Based on this framework, various future studies can advance on-chip acoustic beamforming. First, the theory and techniques developed for optical beamforming, such as the theory on the Gaussian beam [54], can be used to optimize the performance. Second, studies on interfacing the transducer with other acoustic structures, for example, the transition between the focusing and the waveguide sections, and the focusing transducer tailoring for specific waveguide apertures [1], will further improve the proposed structure for applications in various RF microsystems.

V. Conclusion

This work demonstrates gigahertz low-loss unidirectional acoustic focusing transducers using the S0 mode in thin-film $LiNbO_3$. The design considers both the efficient acoustic wave generation and the anisotropic wave propagation. The framework is readily extendable to other acoustic modes. Upon further development, unidirectional focusing transducers can facilitate various RF and cross-domain acoustic microsystems.

Acknowledgment

The authors would like to thank Edmond Chow at the University of Illinois at Urbana–Champaign for his help with microfabrication.

References

[1] A. Siddiqui, R. H. Olsson, and M. Eichenfield, "Lamb wave focusing transducer for efficient coupling to wavelength-scale structures in thin piezoelectric films," *J. Microelectromech. Syst.*, vol. 27, no. 6, pp. 1054–1070, Dec. 2018.

[2] J. B. Green and G. S. Kino, "SAW convolvers using focused interdigital transducers," *IEEE Trans. Sonics Ultrason.*, vol. 30, no. 1, pp. 43–50, Jan. 1983.

[3] J. Z. Wilcox and R. E. Brooks, "Time-Fourier transform by a focusing array of phased surface acoustic wave transducers," *J. Appl. Phys.*, vol. 58, no. 3, pp. 1148–1159, Aug. 1985.

[4] T. J. Marynowski, "Focusing transducer for SAW beamwidth compression on YZ lithium niobate," in *Proc. Ultrason. Symp.*, Oct. 1982, pp. 160–165.

[5] N.-K. Kuo and G. Piazza, "Evidence of acoustic wave focusing in a microscale 630 MHz aluminum nitride phononic crystal waveguide," in *Proc. IEEE Int. Freq. Control Symp.*, Jun. 2010, pp. 530–533.

[6] T.-T. Wu, Y.-T. Chen, J.-H. Sun, S.-C.-S. Lin, and T. J. Huang, "Focusing of the lowest antisymmetric Lamb wave in a gradient-index phononic crystal plate," *Appl. Phys. Lett.*, vol. 98, no. 17, Apr. 2011, Art. no. 171911.

[7] V. Vivek and E. Sok Kim, "Novel acoustic-wave micromixer," in *Proc. IEEE 13th Annu. Int. Conf. Micro Electro Mech. Syst.*, Jan. 2000, pp. 668–673.

[8] V. Laude, D. Gérard, N. Khelfaoui, C. F. Jerez-Hanckes, S. Benchabane, and A. Khelif, "Subwavelength focusing of surface acoustic waves generated by an annular interdigital transducer," *Appl. Phys. Lett.*, vol. 92, no. 9, 2008, Art. no. 094104.

[9] R. Shilton, M. K. Tan, L. Y. Yeo, and J. R. Friend, "Particle concentration and mixing in microdrops driven by focused surface acoustic waves," *J. Appl. Phys.*, vol. 104, no. 1, 2008, Art. no. 014910.

[10] V. Laude, K. Kokkonen, and S. Benchabane, "Characterization of surface acoustic wave focusing by an annular interdigital transducer," in *Proc. IEEE Int. Ultrason. Symp.*, Sep. 2009, pp. 919–922.

[11] S. K. R. S. Sankaranarayanan and V. R. Bhethanabotla, "Numerical analysis of wave generation and propagation in a focused surface acoustic wave device for potential microfluidics applications," *IEEE Trans. Ultrason., Ferroelectr., Freq. Control*, vol. 56, no. 3, pp. 631–643, Mar. 2009.

[12] T.-T. Wu, H.-T. Tang, Y.-Y. Chen, and P.-L. Liu, "Analysis and design of focused interdigital transducers," *IEEE Trans. Ultrason., Ferroelectr., Freq. Control*, vol. 52, no. 8, pp. 1384–1392, Aug. 2005.

[13] Q. Liu, H. Li, and M. Li, "Electromechanical Brillouin scattering in integrated optomechanical waveguides," *Optica*, vol. 6, no. 6, pp. 778–785, 2019.

[14] A. Lawrow, C. N. Pannell, M. Negoita, P. S. J. Russell, and J. Webjörn, "Focused acoustic wave acousto-optic device using a planar domain-inverted lithium niobate transducer," *Opt. Commun.*, vol. 144, nos. 4–6, pp. 161–164, Dec. 1997.

[15] M. M. de Lima, Jr., Alsina, W. Seidel, and P. V. Santos, "Focusing of surface-acoustic-wave fields on (100) GaAs surfaces," *J. Appl. Phys.*, vol. 94, no. 12, pp. 7848–7855, 2003.

[16] W. Jiang *et al.*, "Efficient bidirectional piezo-optomechanical transduction between microwave and optical frequency," *Nature Commun.*, vol. 11, no. 1, pp. 1–7, Dec. 2020.

[17] A. V. Korovin *et al.*, "Conversion between surface acoustic waves and guided modes of a quasi-periodic structured nanobeam," *J. Phys. D, Appl. Phys.*, vol. 52, no. 32, 2019, Art. no. 32LT01.

[18] W. Fu *et al.*, "Phononic integrated circuitry and spin–orbit interaction of phonons," *Nature Commun.*, vol. 10, no. 1, p. 2743, 2019.

[19] S. Maity *et al.*, "Coherent acoustic control of a single silicon vacancy spin in diamond," *Nature Commun.*, vol. 11, no. 1, pp. 1–6, Dec. 2020.

[20] Y. D. Dahmani, C. J. Sarabalis, W. Jiang, F. M. Mayor, and A. H. Safavi-Naeini, "Piezoelectric transduction of a wavelength-scale mechanical waveguide," 2019, *arXiv:1907.13058*. [Online]. Available: http://arxiv.org/abs/1907.13058

[21] D. Taillaert, P. Bienstman, and R. Baets, "Compact efficient broadband grating coupler for silicon-on-insulator waveguides," *Opt. Lett.*, vol. 29, no. 23, pp. 2749–2751, 2004.

[22] A. Mekis *et al.*, "A Grating-Coupler-Enabled CMOS photonics platform," *IEEE J. Sel. Topics Quantum Electron.*, vol. 17, no. 3, pp. 597–608, May 2011.

[23] R. Halir, P. Cheben, S. Janz, D.-X. Xu, Í. Molina-Fernández, and J. G. Wangüemert-Pérez, "Waveguide grating coupler with subwavelength microstructures," *Opt. Lett.*, vol. 34, no. 9, pp. 1408–1410, 2009. [Online]. Available: http://ol.osa.org/abstract.cfm?URI=ol-34-9-1408.

[24] A. Kar, M. Bahadori, S. Gong, and L. L. Goddard, "Realization of alignment-tolerant grating couplers for z-cut thin-film lithium niobate," *Opt. Express*, vol. 27, no. 11, pp. 15856–15867, 2019.

[25] C. S. Hartmann and B. P. Abbott, "Overview of design challenges for single phase unidirectional SAW filters," in *Proc. IEEE Ultrason. Symp.*, Oct. 1989, pp. 79–89.

[26] I. C. Chang, "I. Acoustooptic devices and applications," *IEEE Trans. Sonics Ultrason.*, vol. 23, no. 1, pp. 2–21, Jan. 1976.

[27] M. Pijolat *et al.*, "Large Qxf product for HBAR using smart cut transfer of $LiNbO_3$ thin layers onto $LiNbO_3$ substrate," in *Proc. IEEE Ultrason. Symp.*, Nov. 2008, pp. 201–204.

[28] R. S. Weis and T. K. Gaylord, "Lithium niobate: Summary of physical properties and crystal structure," *Appl. Phys. A, Solids Surf.*, vol. 37, no. 4, pp. 191–203, Aug. 1985.

[29] *IEEE Standard on Piezoelectricity*, ANSI/IEEE Standard 176-1987, 1988.

[30] R. Lu, M.-H. Li, Y. Yang, T. Manzaneque, and S. Gong, "Accurate extraction of large electromechanical coupling in piezoelectric MEMS resonators," *J. Microelectromech. Syst.*, vol. 28, no. 2, pp. 209–218, Apr. 2019.

[31] I. E. Kuznetsova, B. D. Zaitsev, S. G. Joshi, and I. A. Borodina, "Investigation of acoustic waves in thin plates of lithium niobate and lithium tantalate," *IEEE Trans. Ultrason., Ferroelectr., Freq. Control*, vol. 48, no. 1, pp. 322–328, Jan. 2001.

[32] S. Gong and G. Piazza, "Design and analysis of Lithium–Niobate-Based high electromechanical coupling RF-MEMS resonators for wideband filtering," *IEEE Trans. Microw. Theory Techn.*, vol. 61, no. 1, pp. 403–414, Jan. 2013.

[33] R. Wang, S. A. Bhave, and K. Bhattacharjee, "Design and fabrication of s0 Lamb-wave thin-film lithium niobate micromechanical resonators," *J. Microelectromech. Syst.*, vol. 24, no. 2, pp. 300–308, Apr. 2015.

[34] R. Lu, T. Manzaneque, Y. Yang, M.-H. Li, and S. Gong, "Gigahertz low-loss and wideband s0 mode lithium niobate acoustic delay lines," *IEEE Trans. Ultrason., Ferroelectr., Freq. Control*, vol. 66, no. 8, pp. 1373–1386, Aug. 2019.

[35] L. Colombo, A. Kochhar, G. Vidal-Alvarez, and G. Piazza, "X-cut lithium niobate laterally vibrating MEMS resonator with figure of merit of 1560," *J. Microelectromech. Syst.*, vol. 27, no. 4, pp. 602–604, Aug. 2018.

[36] C. J. Sarabalis, Y. D. Dahmani, A. Y. Cleland, and A. H. Safavi-Naeini, "S-band delay lines in suspended lithium niobate," *J. Appl. Phys.*, vol. 127, no. 5, 2020, Art. no. 054501.

[37] R. H. Olsson *et al.*, "A high electromechanical coupling coefficient SH0 Lamb wave lithium niobate micromechanical resonator and a method for fabrication," *Sens. Actuators A, Phys.*, vol. 209, pp. 183–190, Mar. 2014.

[38] M. Kadota, Y. Ishii, and S. Tanaka, "Ultra-wideband T-and π-type ladder filters using a fundamental shear horizontal mode plate wave in a $LiNbO_3$ plate," *Jpn. J. Appl. Phys.*, vol. 58, Jun. 2019, Art. no. SGGC10.

[39] M. Faizan and L. G. Villanueva, "Frequency-scalable fabrication process flow for lithium niobate based Lamb wave resonators," *J. Micromech. Microeng.*, vol. 30, no. 1, 2019, Art. no. 015008.

[40] R. Lu, Y. Yang, M.-H. Li, T. Manzaneque, and S. Gong, "GHz broadband SH0 mode lithium niobate acoustic delay lines," *IEEE Trans. Ultrason., Ferroelectr., Freq. Control*, vol. 67, no. 2, pp. 402–412, Feb. 2020.

[41] T. Manzaneque, R. Lu, Y. Yang, and S. Gong, "Lithium niobate MEMS chirp compressors for near zero power wake-up radios," *J. Microelectromech. Syst.*, vol. 26, no. 6, pp. 1204–1215, Dec. 2017.

[42] M. Kadota, T. Ogami, K. Yamamoto, H. Tochishita, and Y. Negoro, "High-frequency Lamb wave device composed of MEMS structure using $LiNbO_3$ thin film and air gap," *IEEE Trans. Ultrason., Ferroelectr., Freq. Control*, vol. 57, no. 11, pp. 2564–2571, Nov. 2010.

[43] Y. Yang, A. Gao, R. Lu, and S. Gong, "5 ghz lithium niobate MEMS resonators with high FoM of 153," in *Proc. IEEE 30th Int. Conf. Micro Electro Mech. Syst. (MEMS)*, Jan. 2017, pp. 942–945.

[44] R. Lu, Y. Yang, M.-H. Li, M. Breen, and S. Gong, "5-GHz antisymmetric mode acoustic delay lines in lithium niobate thin film," *IEEE Trans. Microw. Theory Techn.*, vol. 68, no. 2, pp. 573–589, Feb. 2020.

[45] V. Plessky, S. Yandrapalli, P. J. Turner, L. G. Villanueva, J. Koskela, and R. B. Hammond, "5 GHz laterally-excited bulk-wave resonators (XBARs) based on thin platelets of lithium niobate," *Electron. Lett.*, vol. 55, no. 2, pp. 98–100, Jan. 2019.

[46] R. T. Schermer and T. H. Stievater, "Millimeter-wave dielectric properties of highly refractive single crystals characterized by waveguide cavity resonance," *IEEE Trans. Microw. Theory Techn.*, vol. 67, no. 3, pp. 1078–1087, Mar. 2019.

[47] I. L. Bajak, A. McNab, J. Richter, and C. D. W. Wilkinson, "Attenuation of acoustic waves in lithium niobate," *J. Acoust. Soc. Amer.*, vol. 69, no. 3, pp. 689–695, Mar. 1981.

[48] R. Lu, T. Manzameque, Y. Yang, and S. Gong, "S0-mode lithium niobate acoustic delay lines with 1 dB insertion loss," in *Proc. IEEE Int. Ultrason. Symp. (IUS)*, Oct. 2018, pp. 1–9.

[49] Y. Yang, R. Lu, L. Gao, and S. Gong, "4.5 GHz lithium niobate MEMS filters with 10% fractional bandwidth for 5G front-ends," *J. Microelectromech. Syst.*, vol. 28, no. 4, pp. 575–577, Aug. 2019.

[50] T. Manzaneque, R. Lu, Y. Yang, and S. Gong, "Low-loss and wideband acoustic delay lines," *IEEE Trans. Microw. Theory Techn.*, vol. 67, no. 4, pp. 1379–1391, Apr. 2019.

[51] B. A. Auld, *Acoustic Fields and Waves in Solids*. Malabar, FL, USA: Krieger Publishing Company, 1990.

[52] A. J. Slobodnik, "Materials and their influence on performance," in *Acoustic Surface Waves*. Berlin, Germany: Springer, 1978, pp. 225–303. [Online]. Available: https://link.springer.com/book/10.1007/3-540-08575-0#about

[53] J. Rodriguez *et al.*, "Direct detection of Akhiezer damping in a silicon MEMS resonator," *Sci. Rep.*, vol. 9, no. 1, p. 2244, Dec. 2019.

[54] B. E. A. Saleh and M. C. Teich, *Fundamentals of Photonics*. Hoboken, NJ, USA: Wiley, 2019.

Ruochen Lu (Member, IEEE) received the B.E. degree (Hons.) in microelectronics from Tsinghua University, Beijing, China, in 2014, and the M.S. and Ph.D. degrees in electrical engineering from the University of Illinois at Urbana–Champaign (UIUC), Urbana, IL, USA, in 2017 and 2019, respectively.

He is currently a Postdoctoral Researcher with UIUC. He will join the Department of Electrical and Computer Engineering, The University of Texas at Austin, Austin, TX, USA, as an Assistant Professor, in January 2021. His research interests include radio frequency microsystems and their applications for timing and signal processing.

Dr. Lu received the Best Student Paper Awards at the 2017 IEEE International Frequency Control Symposium and the 2018 IEEE International Ultrasonics Symposium. He was a recipient of the 2015 Lam Graduate Award, the 2017 Nick Holonyak, Jr., Graduate Research Award, the 2018 Nick Holonyak, Jr., Fellowship, and the 2019 Raj Mittra Outstanding Research Award from the Department of Electrical and Computer Engineering, UIUC.

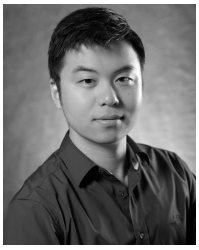

Yansong Yang (Member, IEEE) received the B.S. degree in electrical and electronic engineering from the Huazhong University of Science and Technology, Wuhan, China, in 2014, and the M.S. and Ph.D. degrees in electrical engineering from the University of Illinois at Urbana–Champaign (UIUC), Urbana, IL, USA, in 2017 and 2019, respectively.

He is currently a Postdoctoral Researcher with UIUC. His research interests include design and microfabrication techniques of radio frequency (RF) microelectromechanical systems (MEMS) resonators, filters, switches, and photonic integrated circuits.

Dr. Yang has won the Second Place in the Best Paper Competition at the 2018 IEEE International Microwave Symposium and the Best Paper Award at the 2019 IEEE International Ultrasonics Symposium. He was also a Finalist for the Best Paper Award at the 2018 IEEE International Frequency Control Symposium. He was a recipient of the 2019 P. D. Coleman Graduate Research Award from the Department of Electrical and Computer Engineering, UIUC.

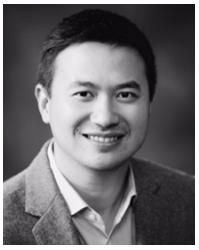

Songbin Gong (Senior Member, IEEE) received the Ph.D. degree in electrical engineering from the University of Virginia, Charlottesville, VA, USA, in 2010.

He is currently an Associate Professor and the Intel Alumni Fellow with the Department of Electrical and Computer Engineering and the Micro and Nanotechnology Laboratory, University of Illinois at Urbana–Champaign (UIUC), Urbana, IL, USA. His primary research interests include design and implementation of radio frequency microsystems, components, and subsystems for reconfigurable radio frequency (RF) front ends. In addition, his research explores hybrid microsystems based on the integration of microelectromechanical systems (MEMS) devices with photonics or circuits for signal processing and sensing.

Dr. Gong is a Technical Committee Member of MTT-21 RF-MEMS of the IEEE Microwave Theory and Techniques Society, the International Frequency Control Symposium, and the International Electron Devices Meeting. He was a recipient of the 2014 Defense Advanced Research Projects Agency Young Faculty Award, the 2017 NASA Early Career Faculty Award, the 2019 UIUC College of Engineer Dean's Award for Excellence in Research, and the 2019 Ultrasonics Early Career Investigator Award. Along with his students and postdoctorals, he received the Best Paper Awards from the 2017 and 2019 IEEE International Frequency Control Symposium, the 2018 and 2019 International Ultrasonics Symposium, and won the Second Place in the Best Paper Competition at the 2018 IEEE International Microwave Symposium. He serves as the Chair of MTT TC2 and TC 21. He also serves an Associate Editor for the IEEE TRANSACTIONS ON ULTRASONICS FERROELECTRICS AND FREQUENCY CONTROL and *Journal of Micrelectromechanical Systems*.